ACS OMEGA

Article

Cite This: ACS Omega 2019, 4, 19145−19152

http://pubs.acs.org/journal/acsodf

Multifunctional Mineral Hydrogels: Potential in Artificially Intelligent Skins and Drug Delivery

Jufen Yan,[†] Jianhua Zhu,*[,‡] Mingfang Cui,[‡] Jing Zhang,[‡] Fang Ma,[‡] Yiping Su,[§] and Xinya Han*[,†]

[†]Department of Chemistry and Chemical Engineering and [‡]Key Laboratory of Metallurgical Emission Reduction & Resources Recycling (Ministry of Education), Anhui University of Technology, Maanshan 243002, China

[§]School of Environmental Science and Engineering, Guangdong Provincial Key Laboratory of Soil and Groundwater Pollution Control, Southern University of Science and Technology, Shenzhen 518055, Guangdong, China

Supporting Information

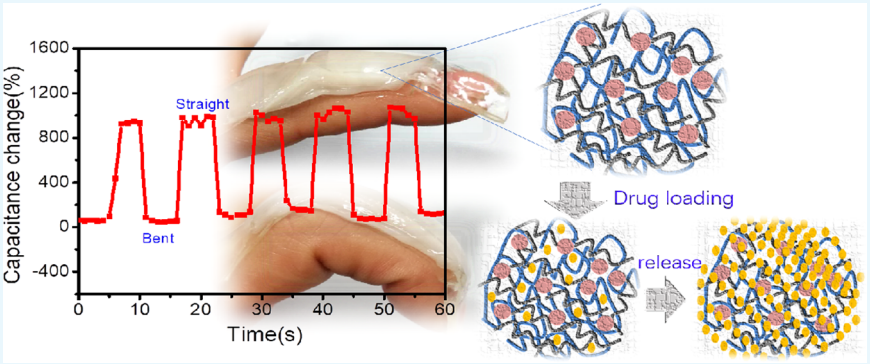

ABSTRACT: Hydrogels have received considerable attention due to their potential applications in the fields of drug delivery, tissue engineering, and stimuli-responsive devices. Nonetheless, it is still a great difficulty in designing hydrogels with multifunctional characteristics including excellent antibacterial activity and appropriate mechanical and remarkable sensing properties. In the present study, a novel type of organic−inorganic adhesive is demonstrated, which comprises inorganic matter of amorphous calcium phosphate particles and organic substances of poly(acrylic acid) and chitosan. The hydrogel possesses excellent biocompatible and antibacterial activity, unique viscoelastic properties, high quantity of drug load, and remarkably sensitive pressure sensing, which have potential use as antibacterial biomaterials, artificially intelligent skins, and drug delivery carriers.

INTRODUCTION

Hydrogels, three-dimensionally interconnected porous polymers, have received extensive attention because of their peculiar properties of high moisture content, hydrophilic nature, softness, and biocompatibility. They have been widely used in biomedical fields, for instance, drug carriers,[1] tissue engineering,[2] wound dressing, and artificial skins under specific environmental stimuli-responsive conditions of pressure, pH,[3] and ionic strength, strain,[4] temperature,[5] humidity,[6] twist deformation,[7] etc.[8] Moreover, their particular structural and mechanical performances can be designed to fulfill specific demands when they are fabricated to the capacitive pressure sensors.[4,9] It is of great significance for hydrogels to be developed and applied in terms of artificial skins with the fast development of artificial intelligence technology. Suo and coworkers developed the polyacrylamide (PAAm) hydrogel sensors with good biocompatibility and stretchability, which could detect a wide strain range from 1 to 500% and measure pressure as low as 1 kPa, widely extending the designability of artificially intelligent skins.[4b] Nevertheless, PAAm hydrogels with chemical crosslinks are short of self-healing ability and have bad intimate surface contact.[4b,10] Wu et al.[9a] reported a mineral hydrogel consisting of amorphous calcium carbonate (ACC) nanoparticles that interacted with poly(acrylic acid) (PAA) and alginates, which could be utilized as a capacitive sensor with recyclable, self-healing, and superior mechanical properties. However, mineral hydrogels suffer from lack of antibacterial activity or antifouling ability and of stability under low pH conditions, which limit their widespread application. It is a big challenge to develop high-performance flexible intelligent skins with combined properties of antibacterial activity, excellent rheological property, and sensitiveness to external stimuli.

Here, we investigated a unique mineral hydrogel with physically crosslinked frameworks of natural polymer chitosan (CS) and poly(acrylic acid) (PAA). Chitosan was chosen because it is a hydrophilic polymer with excellent antimicrobial, biocompatible, and biodegradable properties.[11] The linear

Received: July 31, 2019
Accepted: October 24, 2019
Published: November 6, 2019

DOI: 10.1021/acsomega.9b02435
ACS Omega 2019, 4, 19145−19152

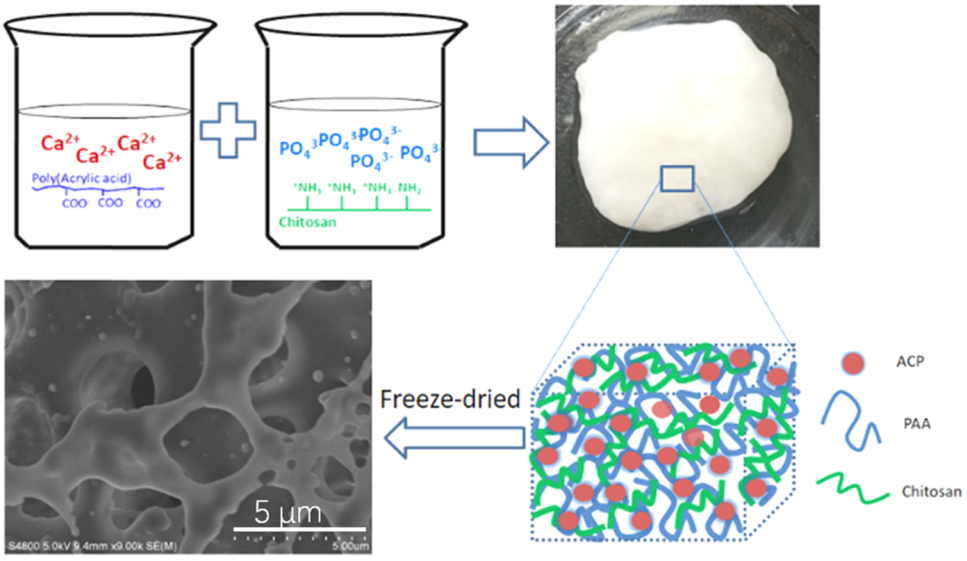

Figure 1. Schematic diagram of ACP/PAA/CS hydrogel formation.

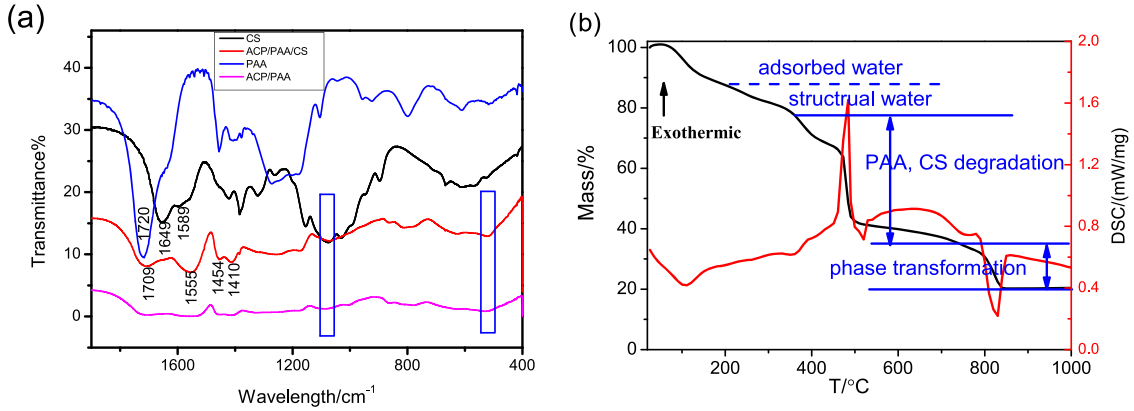

Figure 2. (a) FT-IR spectra for CS, ACP/PAA, and ACP/PAA/CS. (b) Thermogravimetric (TG) and differential scanning calorimetry curves of the ACP/PAA/CS hydrogel.

polysaccharide of each C6 unit contains amino and hydroxyl groups, which is derived from deacetylation of chitin from crustaceans, insects, fungi, etc. Its antimicrobial properties are attributed to the positive charge obtained from the availability of free amino groups in chitosan, which interacts with the bacterial cell membrane.[12]

In consideration of the mentioned concerns and the inspiration of the mineral hydrogel originally from the biomineralization process,[13] a unique organic−inorganic hydrogel with merits of improved pH stability,[14] chitosan producing antibacterial activity, and excellent sensing capability was designed as a novel artificially intelligent skin. As far as we know, there remain few reports about hydrogels with similar multifunctional properties. Herein, the hydrogel was successfully prepared through a facile procedure, which comprises amorphous calcium phosphate (ACP) nanoparticles entrapped within physically crosslinked polymer frameworks. Rheological properties, self-healable and moldable properties, swelling behaviors, drug release, and antibacterial effects of *Escherichia coli* and *Bacillus subtilis* were investigated to develop potential applications in artificially intelligent skins and drug delivery.

RESULTS AND DISCUSSION

Synthesis of an Elastic Compressible Self-Healing Mineral Hydrogel. The ACP/PAA/CS hydrogel was synthesized by introducing $CaCl_2$ solution containing PAA into the solution of Na_2HPO_4 mixed with CS (wt % ≤ 0.1%) under vigorous stirring at ambient conditions (see Experimental Section). The resultant products are white sticky hydrogels (Figure S1a, Supporting Information) with shapeable and self-healing ability. They can be shaped into macroscopic objects with various shapes (Figure S2, Supporting Information). When two hydrogel cylinders with different colors were brought into contact, they would fuse together without any gaps in several minutes (Figure S3, Supporting Information), which implies the excellent self-healing property of hydrogels. However, a higher amount of CS (>0.5 wt %) would result in yellow, tough, nonviscous, and inelastic rubberlike aggregates (Figure S1a, Supporting Information), which do not show self-healing property.

The lyophilized ACP/PAA/CS hydrogel displays interconnected porous microstructures (Figures 1 and S1c). The dry gel could recover quickly within an hour in different solutions (Figure S4, Supporting Information) and maintain the properties as the newly synthesized hydrogels. The dried

DOI: 10.1021/acsomega.9b02435
ACS Omega 2019, 4, 19145−19152

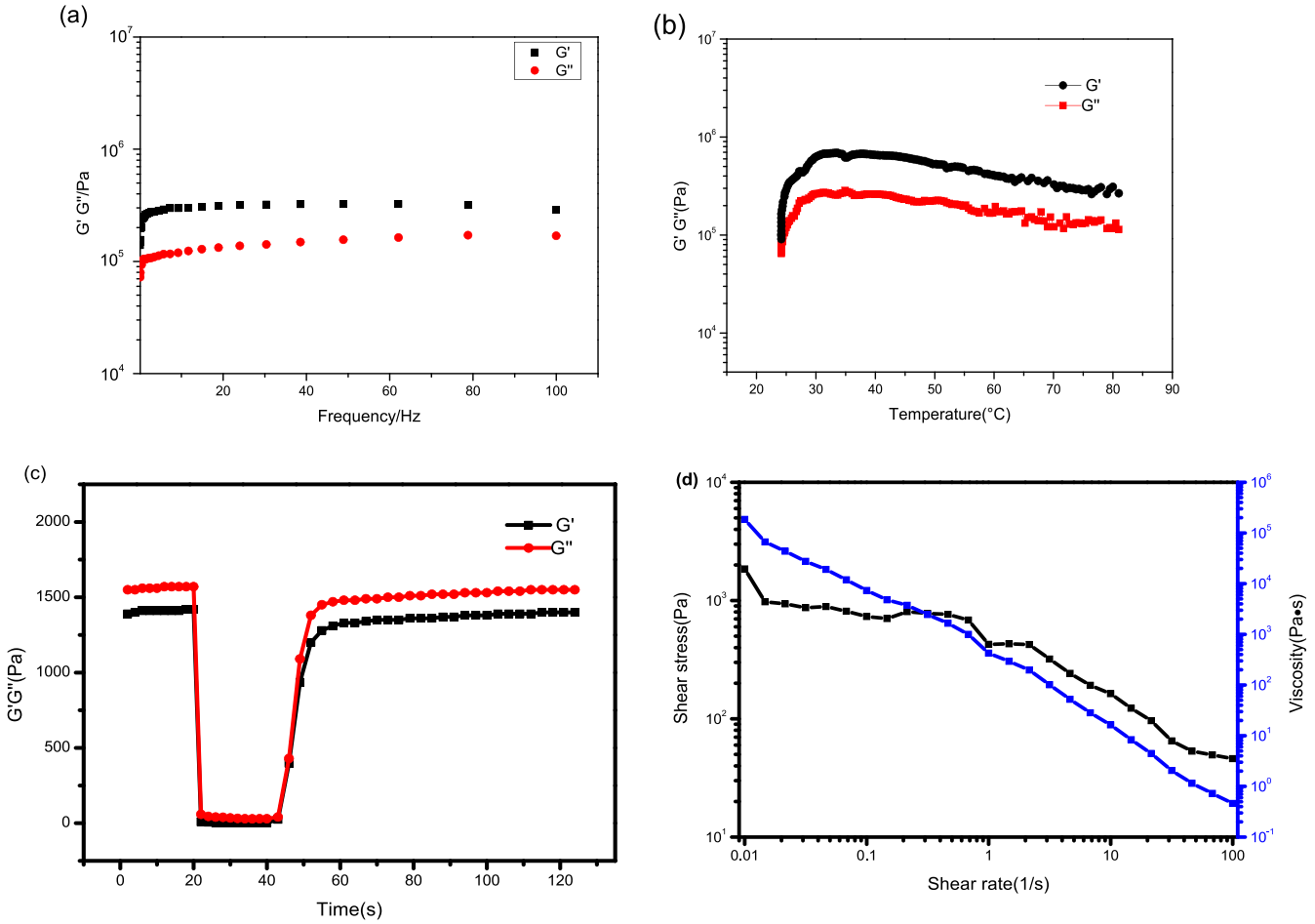

Figure 3. Rheological properties of the ACP/PAA/CS hydrogel. (a, b) Frequency dependencies and temperatures of the storage (G') and loss (G'') moduli; (c) the hydrogel thixotropy; (d) the curve of shear rate and shear stress.

hydrogel sample at 25 °C exhibits fast swelling kinetics in phosphate buffered saline (PBS) (pH = 7.4 and 8.3) and water and reaches maximum swelling ratios of 1.5, 2.75, and 1.7 g/g, respectively, at around 20 min.

The Fourier-transform infrared (FT-IR) spectra of the ACP/PAA/CS hydrogel are displayed in Figure 2a. The peaks at 1068 and 508 cm^{-1} marked with a blue frame are typical phosphate bending vibration attributed to the presence of amorphous calcium phosphate (ACP).[15] The X-ray diffraction pattern of the freeze-dried ACP/PAA/CS hydrogel does not show sharp peaks (Figure S5, Supporting Information), which confirms the amorphous feature of the hydrogel. The peak (Figure 2a) corresponding to the carboxylic group shifts from 1720 cm^{-1} (υ_{COOH}) to 1709 cm^{-1} (υ_{COO^-}), which implies the deprotonation of the COOH groups of PAA molecules. This deprotonation phenomenon was also observed in the ACP/PAA hydrogel synthesized in similar conditions without the CS polymer, suggesting the formation of a Ca^{2+}−COO^- complex in the hydrogel. It was reported that pure Ca^{2+} and PAA molecules (Mw = 100 000) could also produce hydrogels in high pH values.[16] In the current case, the formed ACP particles provide new nodes for the crosslinking of PAA molecules, where deprotonated PAA can interact with Ca^{2+} on the surface of ACP nanoparticles. As CS was also introduced into the hydrogel, new bands were observed for ACP/PAA/CS hydrogels compared with the pure ACP/PAA hydrogel. The FT-IR spectrum reveals that the intensity and shape of amide peaks I and II at 1649 and 1589 cm^{-1}, respectively, in CS have changed significantly in the ACP/PAA/CS hydrogel, producing two new corresponding peaks at 1709 and 1555 cm^{-1} attributed to the COO^- groups in PAA[9a] and the NH_3^+ absorption of CS,[17] respectively. The COO^- groups in PAA can interact with ACP as well as NH_3^+ groups in CS to form crosslinked frameworks through electrostatic interaction in hydrogels. The typical models of ACP/PAA/CS hydrogels can be illustrated in Figure 1, where ACP nanoparticles are trapped within the frameworks of two polymers.

TG measurement of the hydrogel shows a three-stage degradation behavior for the dry hydrogel (Figure 2b). In the first stage, the weight loss of about 23 wt % below 360°C is attributed to the release of free and structural water.[18] The second stage from 361 to 730 °C is the thermal degradation region, which includes the decomposition of CS and PAA. The third step up to 841 °C with a mass loss of 15 wt % is ascribed to the transformation of ACP into the crystalline state. The calculated mass percent of ACP in the dry gel is up to 35 wt %. Thus, the weight ratio of ACP with the polymer and water is about 35:42:23.

Rheological Properties of the ACP/PAA/CS Hydrogel. The rheological characterization of the ACP/PAA/CS hydrogel (Figure 3a) reveals that the storage modulus G' and loss modulus G'' increase with the increase of angular frequency and the former is slightly higher than the latter modulus at 25 °C, which is a typical property of gels with a certain rigid

DOI: 10.1021/acsomega.9b02435
ACS Omega 2019, 4, 19145−19152

structure.[19] The values of both moduli are high, implying the better mechanical strength of the hydrogel.[20] A linear increase in both moduli with increasing frequencies is observed, which is consistent with the Maxwell model. Besides, the hydrogel revealed the representative property of crosslinking materials despite the degree of crosslinking density from both moduli with nonzero limiting values at low frequencies (Figure 3a). The shape of the storage modulus profile is somewhere between typical curves of the polymer with unlinked molecular chains and a soft gel.[19] The rheological data of the ACP/PAA/CS hydrogel show a higher modulus than that of the ACP−PAA hydrogel (Figure S6, Supporting Information), probably due to the increased cohesion strength of new crosslinking between NH_3^+ and COO^- when CS is introduced.

A distinct increase in both G' and G'' (Figure 3b) with an increase in temperature in the range of 25−35 °C and a slight decrease above 35 °C demonstrate the good thermostability and the strong physical crosslinks within the hydrogel under different temperatures. Interestingly, $G' > G''$ occurs during the temperature changes, i.e., the elastic behavior of the hydrogel is changed to the dominant response, which is on account of the reduction of water within the hydrogel. Figure 3c shows that the sample displays fast recovery of mechanical properties after a sharp oscillatory breakdown, called thixotropy. Under the condition of an oscillatory force of 600% at a frequency of 1.0 Hz, the G' value decreases from 1.41 kPa to 6.8 Pa, leading to a solid−liquid state ($\tan\delta = G''/G' = 1.0$). However, when the amplitude is decreased to the initial force ($\gamma = 1\%$) with the same frequency, G' will rapidly recover to the initial value accompanying the sample to a quasi-liquid state ($\tan\delta > 1$), which indicates that the ACP/PAA/CS hydrogel has an excellent self-healing property as verified by the self-healable test (Figure S3, Supporting Information). Figure 3d shows a decrease in stress with increasing shear rates, which is a typical characteristic of the hydrogel.

In Vitro Cell Compatibility and Antibacterial Assay for the ACP/PAA/CS Hydrogel. Good biocompatibility is necessary for well-designed materials in the biomedical field.[21] The in vitro cytocompatibility of the ACP/PAA/CS hydrogel to the normal human dermal fibroblast (NHDF) cells was detected by means of the 3-(4,5-dimethylthiazol-2-yl)-2,5-diphenyltetrazolium bromide (MTT) assay. As displayed in Figure 4, the relative percent cell viability with respect to concentrations of the hydrogel after 24 h was maintained above 99%. Even at high concentrations, the hydrogel did not induce a significant cytotoxic effect. The microscopy images show that there were no obvious differences in the quantity and shape of NHDF cells (Figure S7, Supporting Information). The above results demonstrated that the ACP/PAA/CS hydrogel had no significant influence on the growth of NHDF cells. The low cytotoxicity originates from the good biocompatibility of the hydrogel, which may have promising applications in the biomedical field.

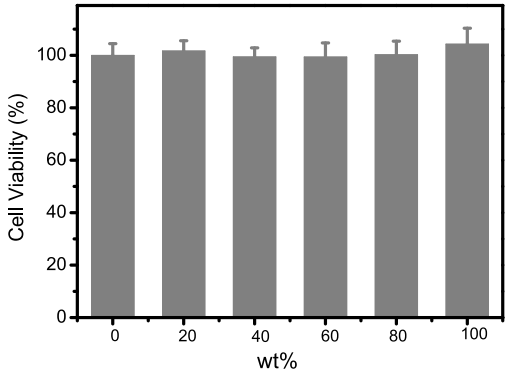

Figure 4. Relative percent cell viability with respect to concentrations of the hydrogel extracts.

Besides serving as a barrier to avoid external bacterial infection, a desired biomedical hydrogel with inherent antibacterial properties will be more promising. In the antibacterial test through the direct contact, both *E. coli* (Gram-negative bacterium) and *B. subtilis* (Gram-positive bacterium) strains were chosen to test the antibacterial activity of the surface ACP/PAA/CS hydrogel. When brought into contact with the hydrogel for 24 h at 37 °C, bacteria treated with 5-cyano-2,3-ditolyl-2H-tetrazolium chloride (CTC) were used to evaluate the respiratory activity of *E. coli*. Live bacteria can metabolize CTC and produce an insoluble and red fluorescent formazan, while dead or unhealthy ones will not reduce CTC.[22] Laser scanning confocal microscopic images showed that few healthy bacteria were observed on the surface of the hydrogel after 24 h of incubation in the bacterial suspension, while plenty of bacteria grew on the contrastive glass surface (Figure 5a,c), combined with about 50% bacterial viability from the quantitative antibacterial efficiency shown in Figure 5c,f, indicating that the hydrogel has excellent inherent antibacterial properties to both *E. coli* and *B. subtilis*. This is mainly ascribed to the positively charged amino groups, which could damage the bacterial walls and destroy the integrity of the cells through electrostatic interactions, causing the release of intracellular matter.[12a,23]

Sustained Release of Kanamycin Sulfate (KS) in Vitro. Most of the hydrogels were shown to be excellent drug carriers due to their porous structure and excellent biocompatibility. Hence, we performed kanamycin sulfate (KS) as a test drug and adsorbed it within the hydrogel to improve the antibacterial activity. The contrast test reveals that ACP/PAA/CS hydrogels are more stable than ACP/PAA hydrogels at acidic pHs or in PBS (7.4) (Figure S9, Supporting Information), which will degrade rapidly (20 min at pH 1.2, 80 min at pH 6.8, and 120 min at pH 7.4; the results are shown in Figure S8, Supporting Information) and cause the burst release of drugs. Obviously, the introduced CS molecules provide more stable frameworks than PAA molecules alone.

The drug KS load can reach a maximum value of 14.1%, based on the standard curve of KS shown (Figure S10, Supporting Information). Meanwhile, the encapsulation efficiency achieves 92.2%. Generally, the drug release from the hydrogel follows the principles of drug diffusion or/and hydrogel degradation. The linear graph between the drug release and time of the system is controlled by polymer erosion, while a parabolic curve between the drug release and time is controlled by drug diffusion.[24] From the release property of KS-loaded ACP/PAA/CS hydrogels at pH 7.4 in vitro (Figure 6), it can be noted that the drug release rates of the ACP/PAA hydrogel and ACP/PAA/CS hydrogel with 0.05% reach 100% within 3 h, which is ascribed to their stability at pH 7.4. The ACP/PAA hydrogel is lost at about 2 h at pH 7.4, and the ACP/PAA/CS hydrogel with 0.05% shows a similar situation at 3 h, resulting in drug release (shown in Figure S8c, Supporting Information). Although the ACP/PAA/CS hydrogel with 0.5% has good stability at pH 7.4, the maximum of the drug cumulative release rate with 70% is lower

DOI: 10.1021/acsomega.9b02435
ACS Omega 2019, 4, 19145−19152

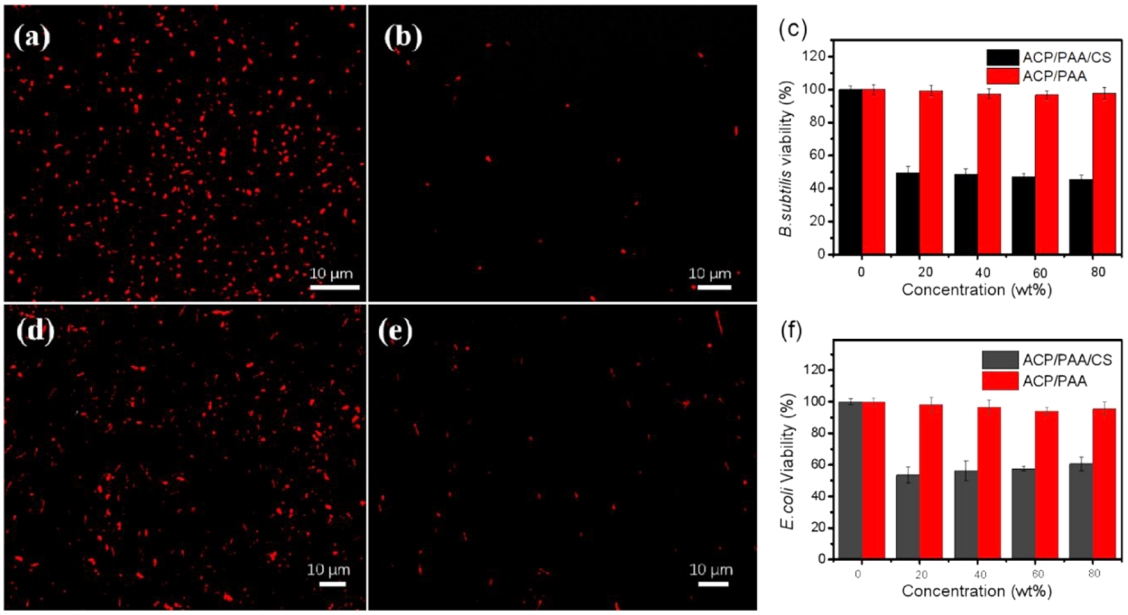

Figure 5. Laser confocal images of *B. subtilis* and *E. coli* on the surface of the ACP/PAA/CS hydrogel after bringing into contact for 24 h. (a) *B. subtilis* on glass as a control. (b) *B. subtilis* on the hydrogel surface. (d) *E. coli* on glass as a control. (e) *E. coli* on the hydrogel surface. (c, f) are the quantitative bacterial viability of *B. subtilis* and *E. coli*, respectively. In both cases, CTC markers were used to distinguish live (red) bacteria.

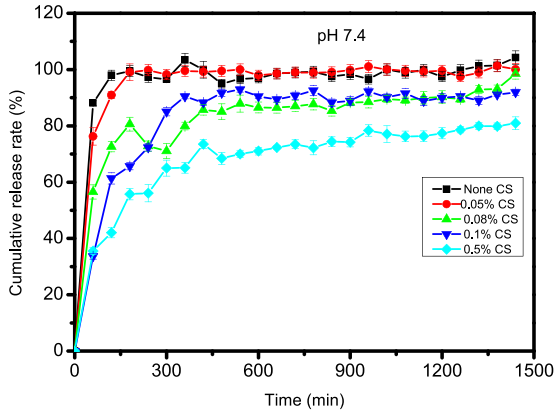

Figure 6. Drug release properties of ACP/PAA/CS and ACP/PAA hydrogels.

than ACP/PAA/CS hydrogels with 0.08 and 0.1% CS that reach 90% for the maximum after 6 h. They both obey a first-order kinetic process with a linear regression of 0.94 during the first 6 h for the complex hydrogel made through the adsorption method. Later, the release rate remains a constant, which indicates that the hydrogels can sustainably release kanamycin sulfate in vitro as a potential drug carrier.

Capacitance of the Hydrogel Sensor. The excellent viscoelasticity, mechanical compliance, and self-healing ability of the prepared hydrogel facilitate the construction of unique artificially intelligent skins. Herein, a capacitive pressure sensor was designed (inset in Figure 7a) according to eq 1[9a]

$$C = \varepsilon S/4\pi kd \quad (1)$$

in which C stands for the capacitance, ε is the dielectric constant of the dielectric layer, k is the electrostatic constant, S is the contacting area of the conducting layer, and d is the distance of the dielectric layer. This was used to measure the capacitance changes of the device as a function of compressive pressure at 0 and 24 h. Its capacitance remains linearly responsive within 5 kPa (Figure 7a). The pressure sensitivity S (the slope of the trace)[25] is 5.264 kPa^{-1}, about 31 times more sensitive than 0.17 kPa^{-1} of the ACC/PAA/alginate hydrogel reported by Wu group.[9a] However, the pressure sensitivity decreased to 0.725 kPa^{-1} with a prolonged time of 24 h (Figure 7b), which is ascribed to the water evaporation of the hydrogel. Therefore, it is important to restrain water evaporation of the hydrogel for better pressure sensitivity.

The durability test of the sensor under a pressure of 1 kPa (Figure 7c,d) indicates the stability of the capacitance–pressure curves for 200 cycles, indicating the high reliability of the ACP/PAA/CS hydrogel device. Based on the character, we assembled a capacitance sensor enveloped by two layers of VHB tape and placed it onto a finger to detect human finger motion (inset in Figure 7d). When the finger bends, the hydrogel deforms severely, resulting in an increase in the capacitance signals. This alternately straightening and bending processes were carried out many times without an obvious loss in the capacitance peak (Figure 7e). Additionally, it can also be applied to monitor the pressure produced by vocal cord vibration if the hydrogel sensor was adhered to the human throat (Figure 7f). All of these properties show that ACP/PAA/CS hydrogels have potential application as extremely sensitive pressure sensors for artificially intelligent skins and wearable devices.

CONCLUSIONS

Briefly, novel ACP/PAA/CS hydrogels composed of ACP particles and macromolecules of PAA and chitosan have been prepared through a facile procedure. The obtained hydrogels possess multiple properties including excellent biocompatibility, self-healing ability, antibacterial activity, good mechanical compliance, and sensing properties for highly sensitive pressure sensing for finger motion. These hydrogels may serve as promising materials as drug carrier vehicles and as artificially intelligent skins, wearable devices, etc.

DOI: 10.1021/acsomega.9b02435
ACS Omega 2019, 4, 19145−19152

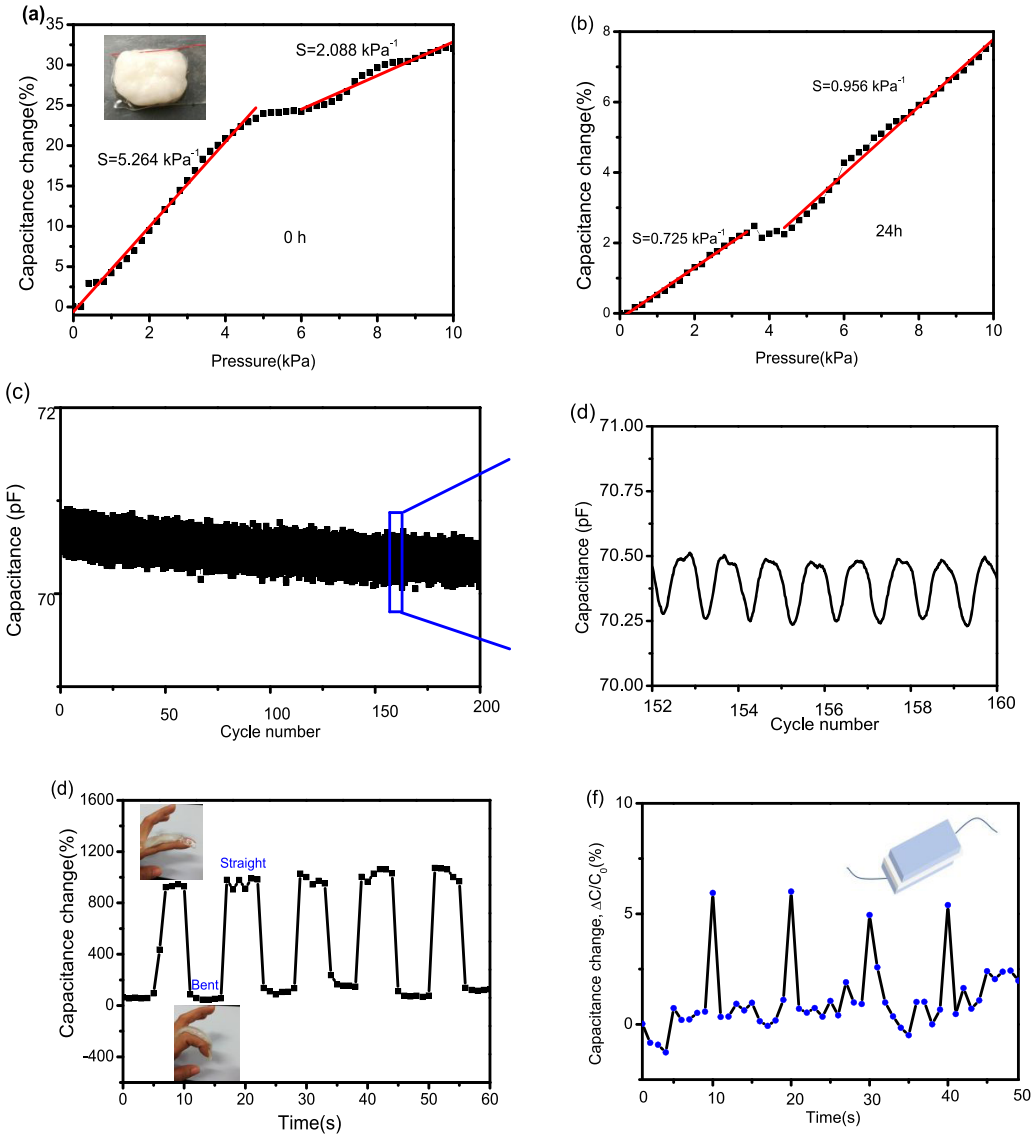

Figure 7. Capacitance−pressure graphs of the pressure sensor from 0 to 10 kPa at 0 h (a) and 24 h (b). (c) Durability of the sensor tested for 200 cycles under a pressure of 1 kPa. (d) Recorded capacitance variations from 152 to 160 cycles. (e) Schematic finger motion hydrogel sensor for finger bending and unbending cyclically for 48 h. (f) Hydrogel pressure sensor served as a flexible sensor for detecting human voice "Ke".

EXPERIMENTAL SECTION

Preparation of the ACP/PAA/CS Hydrogel. A mixed solution of Na_2HPO_4 (0.17 M) and chitosan (0.1 wt %) with 0.1% acetic acid was slowly (3 mL min^{-1}) poured into another solution containing $CaCl_2$ (0.2 M) and poly(acrylic acid) (PAA, 5%, v/v) with stirring. A white sticky hydrogel rapidly formed under the stir bar. After stirring for a few minutes, the turbid solution became clear and then the product was washed with purified water until the last washing water was clear. Hydrogels containing different amounts of CS (0.05, 0.08, and 0.5 wt %) could be prepared via the above procedure. The ACP/PAA hydrogel was prepared in the same way without the introduction of CS.

Swelling Behavior of the Hydrogel. The dry ACP/PAA/CS hydrogel was separately dipped in PBS with different pH (7.4 and 8.3) values at 37 °C. The mass of the wet hydrogels was weighed at 0−260 min with an interval of 20 min during the soaking. The swelling ratio (%) was calculated according to the formula: $(W_i - W_0)/W_0 \times 100\%$, in which W_i is the mass of the swollen hydrogel at every time point and W_0 is the mass of the hydrogel at 0 min.

Cell Culture and Cytotoxicity Test. Cytotoxicity evaluation for the extract of the hydrogel was obtained by means of the MTT assay according to the International Standard ISO 10993-5:2009. The extracts from hydrogels (100, 80, 60, 40, and 20 wt %) were prepared according to the International Standard ISO 10993-12:2012. NHDF cells were used, which were incubated in Dulbecco's modified Eagle medium with 10% fetal bovine serum plus 1% penicillin/streptomycin on 96-well plates (5×10^3 cells/well) in a humidified 5% CO_2 incubator at 37 °C. After 20 h, the media were replaced by fresh growth media containing different concentrations of samples for 24 h. Generally, 20 μL of MTT solution with 5 mg mL^{-1} PBS was pumped into each well of the plate. The NHDF cells were cultivated for another 4 h. Then, 150 μL of dimethyl sulfoxide was added to each well, where the supernatant was discarded. After shaking for 10 min, the plate was measured at 490 nm using a microplate reader (Thermo Fisher Scientific).The cytotoxicity was evaluated

DOI: 10.1021/acsomega.9b02435
ACS Omega 2019, 4, 19145−19152

according to the equation: cell viability% = $A_i/A_c \times 100\%$, in which A_i stands for the absorbance of the sample and A_c means the absorbance of the control.

Load and Release of Kanamycin Sulfate. The freeze-dried hydrogel (0.1 mg) was immerged in a conical flask (100 mL) containing 15 mL of kanamycin sulfate (KS) solution (1 mg mL^{-1}) on a shaking reactor with an agitation speed of 80 rpm at 37 °C for 24 h. Then, the ultraviolet absorbance of KS in the solution was detected at 278 nm by spectrophotometry to calculate its concentration according to the standard curve. Meanwhile, the drug absorbance was also detected after the drug-loading hydrogel was washed twice with distilled water. The drug-loading capicity and encapsulation efficiency were calculated according to the equations: $W_1/W_2 \times 100\%$ and $(W_3 - W_4)/W_3 \times 100\%$, respectively, in which W_1 stands for the mass of KS within the hydrogel, W_2 is the net mass of the hydrogel, W_3 is the total drug mass, and W_4 is the mass of the drug that remained in the solution.

The KS-loaded hydrogels were enclosed in a teabag and introduced in the basket of the drug release apparatus. They were then placed in 150 mL of phosphate buffered saline solution (PBS, pH 7.4) at 37°C, and the basket was stirred at a speed of 50 rpm. Then, 5 mL of the solution was removed at hourly intervals and the amount of KS was analyzed by spectrophotometry. At the same time, 5 mL of fresh PBS solution was periodically added to maintain the original PBS volume.

Bacterial Tests. *E. coli* (ATCC 25922) and *B. subtilis* (ATCC 6633) strains were chosen to detect the antibacterial activity of the hydrogel surface through direct contact. The strains were cultured with Luria–Bertani liquid medium, pH 7.0 in a thermostatic incubator at 37 °C for 20 h. The hydrogels sterilized by UV irradiation were deposited in a 6-well plate containing 2 mL of strains with a density of 8×10^5 CFU mL^{-1} after incubation for 24 h at 37 °C. The control group was carried out with the strain solution being in contact with the glass slides instead of the hydrogel in a similar procedure. After 24 h, CTC was utilized to assess the vitality of the bacteria on the surface of the hydrogel and glass slide. Each sample was observed under a laser scanning confocal microscope (Zeiss LSM 880 microscope, Germany). The optimal excitation/emission wavelength was 450/630 nm.

Capacitance of the Hydrogel Sensor. The dielectric layer (30 μm in thickness) was caught between two layers of hydrogels in connection with two metallic electrodes[9a] (Figure S11, Supporting Information). Moreover, the additional two layers of polyethylene films were put on both sides of the sensor to isolate the sensor and avoid water evaporation. The capacitance–pressure curve of the hydrogel sensor was recorded on a combination of a tensile machine (HY-0230, China) with a deformation rate of 1 mm min^{-1} at 25 °C and an LCR meter (TH2830, China) at an AC voltage of 1 V and a sweeping frequency of 1 kHz. The LCR meter was utilized to detect simultaneous capacitive changes under different stimuli on the device. The pressure sensitivity S could be got from the slope of the traces in the capacitance–pressure curve, $S = \delta(\Delta C/C_0)/\delta p$.[9b]

■ ASSOCIATED CONTENT

Supporting Information

The Supporting Information is available free of charge on the ACS Publications website at DOI: 10.1021/acsomega.9b02435.

List of digital photos; curves; XRD; rheological behavior; microscopy images; other images (PDF)

■ AUTHOR INFORMATION

Corresponding Authors

*E-mail: thesea@ustc.edu.cn. Tel: +86-555-2311879 (J.Z.).
*E-mail: xinyah@126.com (X.H.).

ORCID

Jianhua Zhu: 0000-0002-0937-8873

Notes

The authors declare no competing financial interest.

■ ACKNOWLEDGMENTS

The authors acknowledge the National Natural Science Foundation of China (21571004), the Open Project of Key Laboratory Theoretical Chemistry and Molecule Simulation of Ministry of Education, Hunan University of Science and Technology (LKF1401), and the Natural Science Research Project of Anhui Higher Education Institution (KJ2018A0040) for funding.

■ REFERENCES

(1) (a) Zhao, J.; Zhao, X.; Guo, B.; Ma, P. X. Multifunctional Interpenetrating Polymer Network Hydrogels Based on Methacrylated Alginate for the Delivery of Small Molecule Drugs and Sustained Release of Protein. *Biomacromolecules* **2014**, *15*, 3246–3252. (b) Zhang, L.; Wang, L.; Guo, B.; Ma, P. X. Cytocompatible injectable carboxymethyl chitosan/N-isopropylacrylamide hydrogels for localized drug delivery. *Carbohydr. Polym.* **2014**, *103*, 110–118.

(2) Deng, Z.; Guo, Y.; Zhao, X.; Ma, P. X.; Guo, B. Multifunctional Stimuli-Responsive Hydrogels with Self-Healing, High Conductivity, and Rapid Recovery through Host–Guest Interactions. *Chem. Mater.* **2018**, *30*, 1729–1742.

(3) (a) Liang, Y.; Zhao, X.; Ma, P. X.; Guo, B.; Du, Y.; Han, X. pH-responsive injectable hydrogels with mucosal adhesiveness based on chitosan-grafted-dihydrocaffeic acid and oxidized pullulan for localized drug delivery. *J. Colloid Interface Sci.* **2019**, *536*, 224–234. (b) Qu, J.; Zhao, X.; Ma, P. X.; Guo, B. pH-responsive self-healing injectable hydrogel based on N-carboxyethyl chitosan for hepatocellular carcinoma therapy. *Acta Biomater.* **2017**, *58*, 168–180.

(4) (a) Cohen, D. J.; Mitra, D.; Peterson, K.; Maharbiz, M. M. A highly elastic, capacitive strain gauge based on percolating nanotube networks. *Nano Lett.* **2012**, *12*, 1821–1825. (b) Sun, J. Y.; Keplinger, C.; Whitesides, G. M.; Suo, Z. Ionic skin. *Adv. Mater.* **2014**, *26*, 7608–7614.

(5) (a) Jeon, J.; Lee, H. B. R.; Bao, Z. Flexible wireless temperature sensors based on Ni microparticle-filled binary polymer composites. *Adv. Mater.* **2013**, *25*, 850–855. (b) Webb, R. C.; Bonifas, A. P.; Behnaz, A.; Zhang, Y.; Yu, K. J.; Cheng, H.; Shi, M.; Bian, Z.; Liu, Z.; Kim, Y.-S.; et al. Ultrathin conformal devices for precise and continuous thermal characterization of human skin. *Nat. Mater.* **2013**, *12*, 938–944. (c) Yang, H.; Qi, D.; Liu, Z.; Chandran, B. K.; Wang, T.; Yu, J.; Chen, X. Soft thermal sensor with mechanical adaptability. *Adv. Mater.* **2016**, *28*, 9175–9181.

(6) Chortos, A.; Liu, J.; Bao, Z. Pursuing prosthetic electronic skin. *Nat. Mater.* **2016**, *15*, 937–950.

(7) Lai, Y. C.; Deng, J.; Niu, S.; Peng, W.; Wu, C.; Liu, R.; Wen, Z.; Wang, Z. L. Electric Eel-Skin-Inspired Mechanically Durable and Super-Stretchable Nanogenerator for Deformable Power Source and Fully Autonomous Conformable Electronic-Skin Applications. *Adv. Mater.* **2016**, *28*, 10024–10032.

(8) (a) Hoffman, A. S. Hydrogels for biomedical applications. *Adv. Drug Delivery Rev.* **2012**, *64*, 18–23. (b) Seliktar, D. Designing cell-compatible hydrogels for biomedical applications. *Science* **2012**, *336*, 1124–1128. (c) Hennink, W. E.; van Nostrum, C. F. Novel crosslinking methods to design hydrogels. *Adv. Drug Delivery Rev.*

DOI: 10.1021/acsomega.9b02435
ACS Omega 2019, 4, 19145–19152

2012, *64*, 223−236. (d) Ci, T.; Chen, L.; Yu, L.; Ding, J. Tumor regression achieved by encapsulating a moderately soluble drug into a polymeric thermogel. *Sci. Rep.* **2014**, *4*, No. 5473. (e) Deng, Z.; Hu, T.; Lei, Q.; He, J.; Ma, P. X.; Guo, B. Stimuli-Responsive Conductive Nanocomposite Hydrogels with High Stretchability, Self-Healing, Adhesiveness, and 3D Printability for Human Motion Sensing. *ACS Appl. Mater. Interfaces* **2019**, *11*, 6796−6808.

(9) (a) Lei, Z.; Wang, Q.; Sun, S.; Zhu, W.; Wu, P. A Bioinspired Mineral Hydrogel as a Self-Healable, Mechanically Adaptable Ionic Skin for Highly Sensitive Pressure Sensing. *Adv. Mater.* **2017**, *29*, No. 1700321. (b) Mannsfeld, S. C.; Tee, B. C.; Stoltenberg, R. M.; Chen, C. V. H.; Barman, S.; Muir, B. V.; Sokolov, A. N.; Reese, C.; Bao, Z. Highly sensitive flexible pressure sensors with microstructured rubber dielectric layers. *Nat. Mater.* **2010**, *9*, 859−864.

(10) (a) Yang, C. H.; Chen, B.; Lu, J. J.; Yang, J. H.; Zhou, J.; Chen, Y. M.; Suo, Z. Ionic cable. *Extreme Mech. Lett.* **2015**, *3*, 59−65. (b) Larson, C.; Peele, B.; Li, S.; Robinson, S.; Totaro, M.; Beccai, L.; Mazzolai, B.; Shepherd, R. Highly stretchable electroluminescent skin for optical signaling and tactile sensing. *Science* **2016**, *351*, 1071−1074. (c) Kim, C.-C.; Lee, H.-H.; Oh, K. H.; Sun, J.-Y. Highly stretchable, transparent ionic touch panel. *Science* **2016**, *353*, 682−687. (d) Yang, C. H.; Chen, B.; Zhou, J.; Chen, Y. M.; Suo, Z. Electroluminescence of giant stretchability. *Adv. Mater.* **2016**, *28*, 4480−4484.

(11) (a) Dash, M.; Chiellini, F.; Ottenbrite, R. M.; Chiellini, E. Chitosan-A versatile semi-synthetic polymer in biomedical applications. *Prog. Polym. Sci.* **2011**, *36*, 981−1014. (b) Jayakumar, R.; Menon, D.; Manzoor, K.; Nair, S.; Tamura, H. Biomedical applications of chitin and chitosan based nanomaterials-A short review. *Carbohydr. Polym.* **2010**, *82*, 227−232. (c) Larsson, M.; Huang, W.-C.; Hsiao, M.-H.; Wang, Y.-J.; Nydén, M.; Chiou, S.-H.; Liu, D.-M. Biomedical applications and colloidal properties of amphiphilically modified chitosan hybrids. *Prog. Polym. Sci.* **2013**, *38*, 1307−1328.

(12) (a) Kong, M.; Chen, X. G.; Xing, K.; Park, H. J. Antimicrobial properties of chitosan and mode of action: a state of the art review. *Int. J. Food Microbiol.* **2010**, *144*, 51−63. (b) Badawy, M. E.; Rabea, E. I. A biopolymer chitosan and its derivatives as promising antimicrobial agents against plant pathogens and their applications in crop protection. *Int. J. Carbohydr. Chem.* **2011**, *2011*, 1−29.

(13) (a) Cölfen, H. Biomineralization: a crystal-clear view. *Nat. Mater.* **2010**, *9*, 960−961. (b) Finnemore, A.; Cunha, P.; Shean, T.; Vignolini, S.; Guldin, S.; Oyen, M.; Steiner, U. Biomimetic layer-by-layer assembly of artificial nacre. *Nat. Commun.* **2012**, *3*, No. 966.

(14) Xia, M.; Meng, Z.; Zhu, M. Design and fabrication of novel organic/inorganic thermoresponsive hydrogels with excellent mechanical properties. *Mater. Res. Innovations* **2015**, *19*, S15−S19.

(15) (a) Wang, H.; Li, W.; Lu, Y.; Wang, Z. Studies on chitosan and poly(acrylic acid) interpolymer complex. I. Preparation, structure, pH-sensitivity, and salt sensitivity of complex-forming poly(acrylic acid): Chitosan semi-interpenetrating polymer network. *J. Appl. Polym. Sci.* **2015**, *65*, 1445−1450. (b) Yao, K. D.; Peng, T.; Goosen, M. F. A.; Min, J. M.; He, Y. Y. pH-sensitivity of hydrogels based on complex forming chitosan: Polyether interpenetrating polymer network. *J. Appl. Polym. Sci.* **1993**, *48*, 343−354.

(16) Schupp, D. J.; Zhang, X.; Sun, S.; Cölfen, H. Mineral plastic hydrogels from the cross-linking of polyacrylic acid and alkaline earth or transition metal ions. *Chem. Commun.* **2019**, *55*, 4913−4916.

(17) Hu, Y.; Jiang, X.; Ding, Y.; Ge, H.; Yuan, Y.; Yang, C. Synthesis and characterization of chitosan-poly(acrylic acid) nanoparticles. *Biomaterials* **2002**, *23*, 3193−3201.

(18) Mucha, M.; Pawlak, A. Thermal analysis of chitosan and its blends. *Thermochim. Acta* **2005**, *427*, 69−76.

(19) Mezger, T. G. The Rheology Handbook, 4th edition. Hanover, Germany, 2014.

(20) Bhatnagar, D.; Xu, D.; Gersappe, D.; Rafailovich, M. H. Hyaluronic Acid and Gelatin Clay Composite Hydrogels: Substrates for Cell Adhesion and Controlled Drug Delivery. *J. Chem. Biol. Interfaces* **2014**, *2*, 34−44.

(21) Qu, J.; Zhao, X.; Liang, Y.; Zhang, T.; Ma, P. X.; Guo, B. Antibacterial adhesive injectable hydrogels with rapid self-healing, extensibility and compressibility as wound dressing for joints skin wound healing. *Biomaterials* **2018**, *183*, 185−199.

(22) Phoeung, T.; Spanedda, M. V.; Roger, E.; Heurtault, B.; Fournel, S.; Reisch, A.; Mutschler, A.; Perrin-Schmitt, F.; Hemmerlé, J.; Collin, D.; Rawiso, M.; Boulmedais, F.; Schaaf, P.; Lavalle, P.; Frisch, B. Alginate/Chitosan Compact Polyelectrolyte Complexes: A Cell and Bacterial Repellent Material. *Chem. Mater.* **2017**, *29*, 10418−10425.

(23) Bautista-Baños, S.; Hernández-Lauzardo, A. N.; Velázquez-del Valle, M. G.; Hernández-López, M.; Barka, E. A.; Bosquez-Molina, E.; Wilson, C. L. Chitosan as a potential natural compound to control pre and postharvest diseases of horticultural commodities. *Crop Prot.* **2006**, *25*, 108−118.

(24) Kim, C. J. Release kinetics of coated, donut-shaped tablets for water soluble drugs. *Eur. J. Pharm. Sci.* **1999**, *7*, 237−242.

(25) Mannsfeld, S. C.; Tee, B. C.; Stoltenberg, R. M.; Chen, C. V.; Barman, S.; Muir, B. V.; Sokolov, A. N.; Reese, C.; Bao, Z. Highly sensitive flexible pressure sensors with microstructured rubber dielectric layers. *Nat. Mater.* **2010**, *9*, 859−864.

DOI: 10.1021/acsomega.9b02435
ACS Omega 2019, 4, 19145−19152